Electronic Materials Letters (2020) 16:174–179
https://doi.org/10.1007/s13391-019-00193-0

ORIGINAL ARTICLE - ENERGY AND SUSTAINABILITY

Intercorrelated Relationship Between the Thermoelectric Performance and Mechanical Reliability of Mg_2Si-Reduced Graphene Oxide Nanocomposites

Gwansik Kim[1] · Wonkyung Kim[2] · Wooyoung Lee[1]

Received: 3 September 2019 / Accepted: 13 December 2019 / Published online: 1 January 2020

Abstract

We fabricated Mg_2Si-based thermoelectric nanocomposites with reduced graphene oxide using ultrasonic-based wet chemical pulverizing-mixing and spark plasma sintering to improve the trade-off relationship between thermoelectric properties and mechanical reliability. The dependence of thermoelectric properties and mechanical reliability on the nanophase morphologies has been systemically investigated, demonstrating the fracture toughness of the nanocomposite with thin reduced graphene oxide significantly increased. Moreover, the introduction of the few-layered reduced graphene oxide with high interface density was more effective in improving the trade-off relationship. This result suggests that an in-depth research on the dependence of the thermoelectric properties and mechanical reliability on the intrinsic properties of the nanophases is required to prepare efficient thermoelectric nanocomposites.

Graphic Abstract

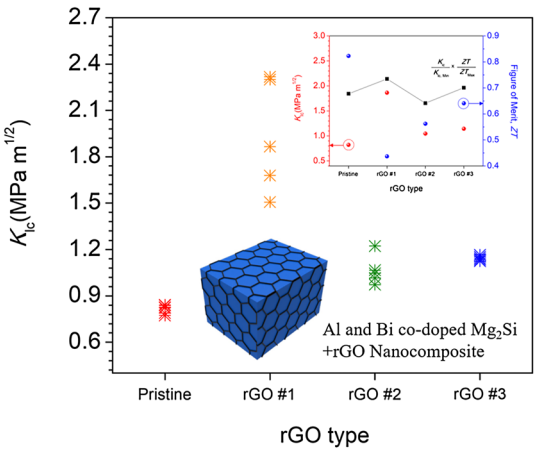

Keywords Thermoelectric · Mg_2Si · Fracture toughness · Trade-off relationship

✉ Wonkyung Kim
happ20@daum.net

✉ Wooyoung Lee
wooyoung@yonsei.ac.kr

[1] Department of Materials Science and Engineering, Yonsei University, Seoul 03722, Republic of Korea

[2] School of Nano and Materials Science and Engineering, Kyungpook National University, 2559 Gyeongsang-daero, Daegu, Gyeongsangbuk-do 37224, Republic of Korea

1 Introduction

Thermoelectric power generators (TEGs) have attracted worldwide attention as new energy conversion technologies that can help reducing carbon emissions (causing serious environmental problems by using fossil fuels). In particular, magnesium silicide (Mg_2Si)-based compounds are promising candidates for automotive thermoelectric generators

(ATEGs) owing to their relatively high thermoelectric (TE) figure of merit ($ZT = \sigma S^2 T/\kappa_{tot}$, where σ is the electrical conductivity, S is the Seebeck coefficient, T is absolute temperature, and κ_{tot} is the total thermal conductivity) for middle–high ranges of temperature. Mg_2Si-based compounds have further advantages for ATEGs such as non-toxicity, low density, and low cost. Hence, several investigations have focused on the improvement in the ZT of Mg_2Si by doping the Si-sites (with Bi or Sb) and Mg-sites (with Al), using Mg_2Sn and Mg_2Ge solid solutions, and introducing nanophases [1–7]. As a result, the maximum ZT of the Mg_2Si was determined to be ~ 1.2 at 770 K on a lab scale [8].

Despite the high ZT value, the low mechanical reliability (fracture toughness, $K_{Ic} \sim 0.82$) of Mg_2Si limits its application to silicide-based TE modules [9]. The large temperature difference between the two electrodes of the TE module under the ATEG operating conditions generally induces thermal and mechanical stress in the TE materials, leading to a breakdown of the TE module electric circuit. The relation between the TE and mechanical properties of Mg_2Si should be verified to ensure the reliability of the TE module. However, few systematic researches have addressed this issue so far. In our previous reports, the ZT and the K_{Ic} of nanocomposites incorporating various nanophases (e.g., metal nanoparticles, reduced graphene oxides (rGOs), and dual nanoinclusions) were introduced [9–12]. We demonstrated the occurrence of a strong trade-off relationship between the ZT and the K_{Ic} of Mg_2Si-based TE nanocomposites, strongly dependent on the interface density.

Herein, we characterized the TE properties and the K_{Ic} of $Mg_{1.96}Al_{0.04}Si_{0.97}Bi_{0.03}$ bulk nanocomposites. These were prepared by introducing commercialized two-dimensional rGOs, having different thicknesses and surface areas, by ultrasonic-based wet chemical pulverizing-mixing process. Furthermore, we systemically investigated TE and mechanical properties and microstructure of the nanocomposites, revealing a strong intercorrelation between their TE or mechanical properties and the rGOs' morphologies.

2 Experiment

We fabricated bulk nanocomposites of $Mg_{1.96}Al_{0.04}Si_{0.97}Bi_{0.03}$ by introducing three types of commercialized few-layered rGOs having different thicknesses and surface areas, with the aim of investigating their TE and mechanical properties in relation to the rGOs' morphologies. $Mg_{1.96}Al_{0.04}Si_{0.97}Bi_{0.03}$ powders were prepared using the up-scaled solid-state reaction technique [13]. The commercialized rGOs used in this study are shown in Table 1. Subsequently, we prepared hybrid powders of $Mg_{1.96}Al_{0.04}Si_{0.97}Bi_{0.03}$ and rGOs by ultrasonic-based wet chemical pulverizing-mixing process at a large scale (10 g/batch), as described in our previous study [11].

Table 1 Thicknesses and surface areas of the commercialized rGOs

	Thickness (nm)	Surface area (m^2/g)
rGO #1	< 1	400–800
rGO #2	10–20	< 21
rGO #3	1–20	50–80

The polycrystalline bulks (25 mm in diameter and 3 mm in thickness) were compacted by spark plasma sintering (SPS) at 1023 K for 5 min under 70 MPa in a vacuum. The microstructure of hybrid powders was observed using a scanning electron microscope (SEM, JEOL-7800F, JEOL Ltd., Japan). The electrical conductivity (σ) and the Seebeck coefficient (S) at 300–873 K were measured using a Seebeck coefficient and electric resistance measuring system (Ulvac ZEM-3, Japan) in He atmosphere. The Hall measurement of the nanocomposites was performed using a home-made system under a 1 T magnetic field in the van der Pauw configuration. The carrier concentration (n_c) and mobility (μ_{Hall}) were estimated using the one-band model. The total thermal conductivity (κ_{tot}) was calculated based on the equation $\kappa_{tot} = \rho_s C_p \lambda$, where ρ_s is the density, C_p is the specific heat capacity, and λ is the thermal diffusivity. The thermal diffusivity (λ) at 373–873 K was measured by the laser flash method (Netszch LFA-457, Germany) under a vacuum. The specific heat capacity (C_p) was measured by differential scanning calorimetry (DSC 8000, Perkin Elmer, USA).

The fracture toughness (K_{Ic}) was obtained by the following equation:

$$K_{Ic} = \chi \left(\frac{E}{H}\right)^{1/2} \frac{P}{a^{3/2}}$$

where P is the applied load, E is the Young's modulus, H is the Vickers hardness, a is the radial crack length measured from the center of the indent, and χ is a calibration constant taken to be 0.016 ± 0.004 [14]. The Vickers hardness and the radial crack length were measured by a Vickers hardness tester (Mitutoyo_HM-101, Mitutoyo, Japan), with a load of 2.942 N and a dwell time of 10 s.

3 Results and Discussion

The introduction of low-dimensional carbon-based nanomaterials [e.g., graphene, rGOs, and carbon nanotubes (CNTs)] is a promising strategy to improve TE properties: the intensified phonon scattering at their interfaces effectively reduces the lattice thermal conductivity [15–18]. Due to their characteristics (e.g., large surface area, high aspect ratio, and high mechanical properties) these carbon-based

nanomaterials have also been widely used as nanofillers to enhance the mechanical reliability of composite materials [19]. In this regard, we fabricated Mg_2Si-based TE nanocomposites with rGOs having different surface areas, aspect ratios, and thicknesses in order to simultaneously increase their TE and mechanical properties. The SEM images in Fig. 1 show the $Mg_{1.96}Al_{0.04}Si_{0.97}Bi_{0.03}$ powders mixed with various types of rGOs. It is observed that well-controlled and dispersed rGOs are present in the form of wrapped or decorated onto the $Mg_{1.96}Al_{0.04}Si_{0.97}Bi_{0.03}$ powders. After mixing, the thickness of the rGOs was similar to their original thickness. Figure 1a shows that rGO #1 was thinner, had a larger surface area, and was evenly monodispersed on the $Mg_{1.96}Al_{0.04}Si_{0.97}Bi_{0.03}$ powders (see the black arrows in Fig. 1a). On the contrary, Fig. 1b, c show rGOs having their original thickness, suggesting no chemical or physical changes during the wet chemical mixing process.

Figure 2a, b show the temperature dependences of σ and S in the sintered samples for various types of rGOs. The σ values of the nanocomposites mixed with all the rGO types were lower compared to that of the pristine sample, within the whole measured temperature range. It should be noted that the nanocomposites dispersed with rGO #1 had the lowest σ among all samples. This result is inconsistent with the fact that the presence of rGOs at the grain boundaries generally improves the electronic transport properties of TE materials. However, in our experiments, the introduction of the rGOs has the effect of lowering the electrical transport properties. To clarify why the dispersed rGOs negatively affected the electrical transport in $Mg_{1.96}Al_{0.04}Si_{0.97}Bi_{0.03}$, we calculated the n_c and μ_{Hall} values based on the one-band model. The corresponding results are presented in Table 2. For all the nanocomposites with rGOs, the n_c value ($n_c = 8.24 \times 10^{18}$–$7.83 \times 10^{19}$ cm^{-3}) decreased significantly, due to the charge compensation induced by the introduction of rGOs. The μ_{Hall} values changed differently: the nanocomposites with rGOs #2 and #3 showed reduced μ_{Hall} values, due to the intensified electron scattering at the interface between the matrix and the rGOs, whereas the nanocomposite with rGO #1 showed increased μ_{Hall} values. The enhanced μ_{Hall} of the nanocomposite with rGO #1 can be attributed to a negligible schottky barrier by the introduction of the rGO at the grain boundaries, or to a dominant conduction through the rGO path despite the similar mean free paths (~ 20 nm) of the electrons and phonons [20, 21].

The absolute values of S in the nanocomposites showed the trade-off relationship with the n_c values. The nanocomposites with rGO #1 had a higher S values, accompanied by a significant decrease in n_c. However, the increase in S was not significant compared to the decrease in n_c: in Mg_2Si-based TE materials, the trade-off relationship between S and n_c is unfavorable, due to the narrow optimized n_c range with a high power factor [11]. This explains why all the nanocomposites had lower power factors compared to the pristine sample. Overall, these results demonstrate that the electronic transport parameter of the basic matrix and the intrinsic properties of the nanophase should be considered simultaneously for improving the TE properties.

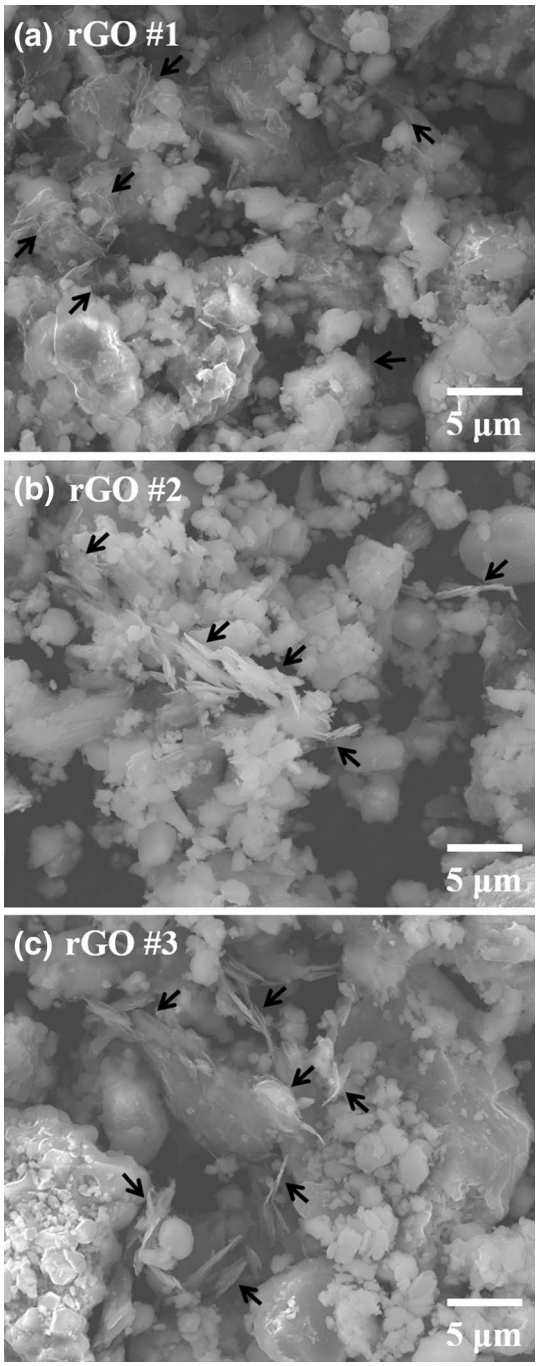

Fig. 1 SEM images of the hybrid powders of $Mg_{1.96}Al_{0.04}Si_{0.97}Bi_{0.03}$ and 3 vol% rGOs

The temperature dependences of κ_{tot} for each rGO type are shown in Fig. 3a. The κ_{tot} values (3.82–4.89 W m^{-1} K^{-1}

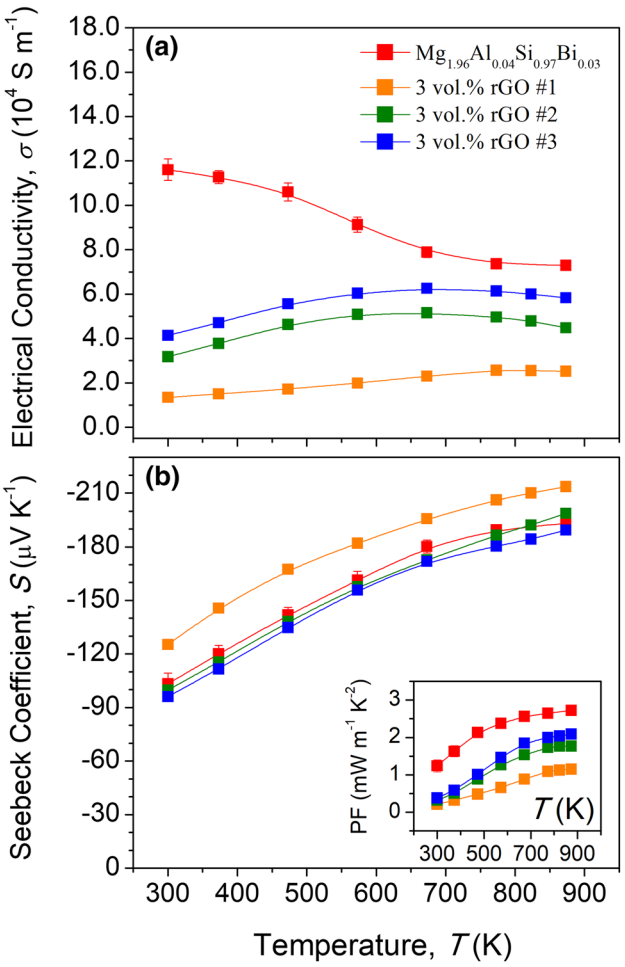

Fig. 2 Temperature dependences of **a** the electrical conductivity and **b** the Seebeck coefficient for all the rGO nanocomposites. The inset in **b** shows the temperature dependence of the power factor

at 373 K; 2.30–2.85 W m^{-1} K^{-1} at 873 K) of the nanocomposites with rGO were lower than those of the pristine sample (5.06 W m^{-1} K^{-1} at 373 K; 2.89 W m^{-1} K^{-1} at 873 K) for the whole measured temperature range. The nanocomposite with rGO #1 presented a significantly lower κ_{tot} value than the other nanocomposites. To clarify the scattering mechanism, we calculated the lattice thermal conductivity (κ_{lat}), as shown in the inset of Fig. 3b. The κ_{lat} value was estimated by subtracting the electronic contribution κ_{ele} ($=L\sigma T$, where L is the Lorenz number) from κ_{tot}. The L values was calculated using the following equation [22]:

$$L = \left(\frac{k_B}{e}\right)^2 \left\{ \frac{\left(r+7/2\right)F_{r+5/2}(\eta)}{\left(r+3/2\right)F_{r+1/2}(\eta)} - \left[\frac{\left(r+5/2\right)F_{r+3/2}(\eta)}{\left(r+3/2\right)F_{r+1/2}(\eta)} \right]^2 \right\},$$

where η is the Fermi energy, $F_n(\eta)$ is the nth order Fermi integral, and r is the scattering parameter. L was equal to ~ 2.44×10^{-8} V^2 K^{-2}. The κ_{lat} values of the samples were not significantly different among each other, suggesting that the offset effect between the intensified phonon scattering at the interfaces and an increased thermal conduction due to the high κ of the rGOs. Thick rGOs cannot work as an effective phonon scattering sources, due their intrinsically high κ. Therefore, the rGO #1 nanocomposite with relatively thinner rGO presented a lower κ_{lat} value compared to the other nanocomposites. However, the trend of the κ_{lat} values ($1/T$ dependence of κ_{lat}) changed at high temperatures (> 673 K), indicating that the hole generation cause an increase in the bipolar contribution (κ_{bp}) [12].

The ZT values calculated from the measured σ, S, and κ_{tot} are presented in Fig. 3b. The introduction of the commercialized rGOs deteriorated the TE performance of the nanocomposites, due to their unfavorable electronic and thermal transport properties. The commercialized rGO nanocomposites showed lower ZT values (0.44–0.64 at 873 K) than that of the pristine $Mg_{1.96}Al_{0.04}Si_{0.97}Bi_{0.03}$ sample (0.82 at 873 K), mainly due to a decrease in the power factor.

ZT values and mechanical reliability are both important for the application of TE materials. For this reason, the K_{Ic} values of the nanocomposites were also investigated; the corresponding results are presented in Fig. 4. We repeated the K_{Ic} measurements 5 times at different points over the surface in order to obtain the reliability of the results. Notably, the K_{Ic} of the nanocomposites (1.05–1.87 MPa m$^{1/2}$) was higher than that of the pristine sample (~ 0.82 MPa m$^{1/2}$). The K_{Ic} enhancement mechanisms (i.e., the deflection of crack propagation, crack bridging, and sheet pull-out within the crack) were apparently activated in the nanocomposites [11]. However, the enhancement of the K_{Ic} in the nanocomposites with thick rGOs (i.e., #2 and #3) was insufficient, due to the low interface density and bulk properties

Table 2 Electronic transport parameters of all the rGO nanocomposites at room temperature

	σ (S m^{-1})	S (μV K^{-1})	n_c (cm^{-3})	μ_{Hall} (cm^2 V^{-1} s^{-1})
$Mg_{1.96}Al_{0.04}Si_{0.97}Bi_{0.03}$	1.23×10^5	−99.78	9.27×10^{19}	81.4
$Mg_{1.96}Al_{0.04}Si_{0.97}Bi_{0.03}$ + 3 vol% rGO #1	0.13×10^5	−125.27	8.24×10^{18}	100.3
$Mg_{1.96}Al_{0.04}Si_{0.97}Bi_{0.03}$ + 3 vol% rGO #2	0.32×10^5	−99.78	7.35×10^{19}	26.6
$Mg_{1.96}Al_{0.04}Si_{0.97}Bi_{0.03}$ + 3 vol% rGO #3	0.41×10^5	−96.11	7.83×10^{19}	32.5

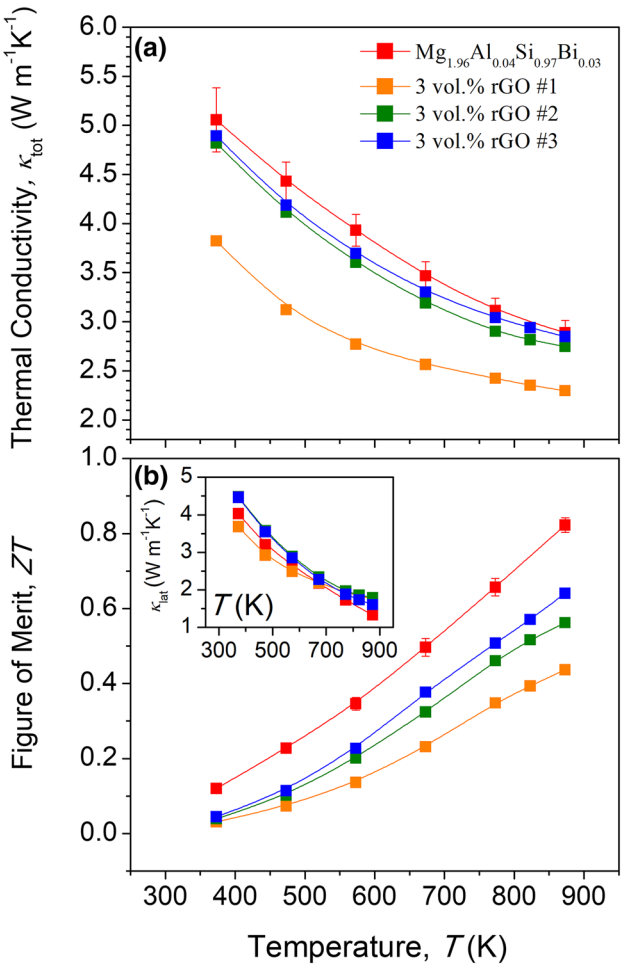

Fig. 3 Temperature dependences of **a** the total thermal conductivity and **b** the *ZT* for all the rGO nanocomposites. The inset in **b** shows the temperature dependence of the lattice thermal conductivity

of carbon. The morphology of the grains wrapped by the rGOs promoted the two-dimensional propagation of cracks, likely interfering with their three-dimensional propagation and increasing the K_{Ic} value. Since the thinner rGO was not punctured or penetrated, crack propagation was likely deflected around it, and sheet pull-out and crack bridging could be expected to interfere with crack propagation by absorbing its energy. Sheet pull-out requires more energy than fiber pull-out; these could have been equally applied to the crack bridging effect, due to an increase in the contact area with the matrix [19]. Apparently, the K_{Ic} values of the nanocomposites greatly depended on the microstructure of the hybrid powder.

The *ZT* and K_{Ic} values of the nanocomposites were compared by calculating $\frac{K_{Ic}}{K_{Ic,\,Min}} \times \frac{ZT}{ZT_{Max}}$: this operation can be an indicator of the TE application because it provides a numerical value for the quantitative evaluation of the trade-off relationship, although the physical meaning is not significant. As shown in Fig. 5, we represented the values of K_{Ic}, *ZT*, and the $\frac{K_{Ic}}{K_{Ic,\,Min}} \times \frac{ZT}{ZT_{Max}}$ factor for each rGO type. The highest $\frac{K_{Ic}}{K_{Ic,\,Min}} \times \frac{ZT}{ZT_{Max}}$ value was obtained for the nanocomposite with rGO #1, mainly due to its significantly higher K_{Ic}. Although we observed a deterioration of the TE properties with the introduction of the commercialized few-layered rGOs, the trade-off relationship between *ZT* and K_{Ic} slightly improved. Our results highlight the necessity of investigating the trade-off relationship between the *ZT* and K_{Ic} values of the TE bulks, in order to fabricate the high efficient TE module and system. Moreover, we emphasized how the morphology of the rGOs is an important factor to consider when preparing bulk TE nanocomposites with improved trade-off relationship.

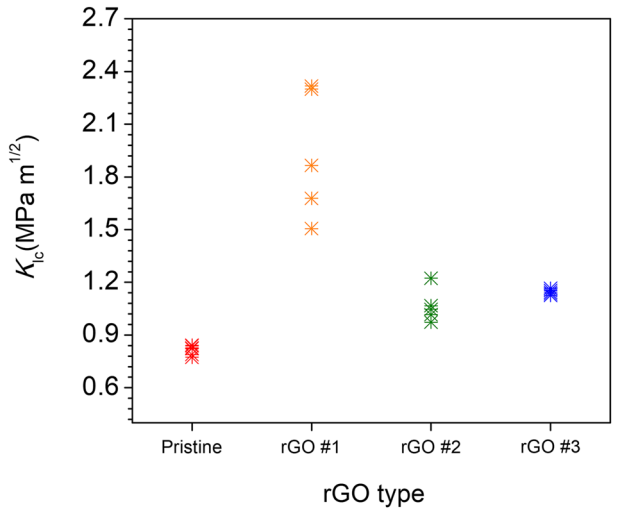

Fig. 4 Fracture toughness for all the rGO nanocomposites

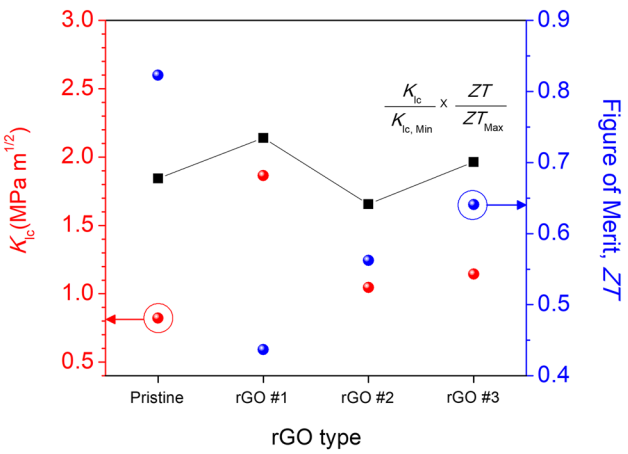

Fig. 5 Fracture toughness, *ZT*, and $\frac{K_{Ic}}{K_{Ic,\,Min}} \times \frac{ZT}{ZT_{Max}}$ values for all the rGO nanocomposites

4 Conclusions

We developed Mg_2Si-based TE nanocomposites with an improved trade-off relationship between their TE properties and mechanical reliability. The rGO morphologies had a great influence on the TE properties and on the fracture toughness of these nanocomposites. Although a reduction of the *ZT* (0.44 at 873 K) was observed for the nanocomposite with thin rGO, its fracture toughness significantly increased (1.87 MPa $m^{1/2}$). Moreover, we found that the optimization of the power factor is required by optimizing the carrier concentration and minimizing the electron scattering in Mg_2Si-based TE nanocomposites. Overall, our experiments proved that the introduction of an optimum amount of nanophases with optimum morphologies would allow the fabrication of nanocomposites with optimized trade-off relationship.

Acknowledgements This work was supported by the National Research Foundation of Korea (NRF) Grant (2017R1A2A1A17069528) and Basic Science Research Program funded by the Korea government (MSIT) and the Ministry of Education (NRF-2019R1A6A1A11055660).

References

1. Tani, J., Kido, H.: Thermoelectric properties of Bi-doped Mg_2Si semiconductors. Phys. B **364**, 218 (2005)
2. Tani, J., Kido, H.: Thermoelectric properties of Sb-doped Mg_2Si semiconductors. Intermetallics **15**, 1202 (2007)
3. Battiston, S., Fiameni, S., Saleemi, M., Boldrini, S., Famengo, A., Agresti, F., Stingaciu, M., Toprak, M.S., Fabrizio, M., Barison, S.: Synthesis and characterization of Al-doped Mg_2Si thermoelectric materials. J. Electron. Mater. **42**, 1956 (2013)
4. Kim, G., Kim, J., Lee, H., Cho, S., Lyo, I., Noh, S., Kim, B.W., Kim, S.W., Lee, K.H., Lee, W.: Co-doping of Al and Bi to control the transport properties for improving thermoelectric performance of Mg_2Si. Scr. Mater. **116**, 11 (2016)
5. Zhang, Q., He, J., Zhu, T.J., Zhang, S.N., Zhao, X.B., Tritt, T.M.: High figures of merit and natural nanostructures in $Mg_2Si_{0.4}Sn_{0.6}$ based thermoelectric materials. Appl. Phys. Lett. **93**, 102109 (2008)
6. Farahi, N., Prabhudev, S., Botton, G.A., Zhao, J., Tse, J.S., Liu, Z., Salvador, J.R., Kleinke, H.: Local structure and thermoelectric properties of $Mg_2Si_{0.977-x}Ge_xBi_{0.023}$ ($0.1 \leqslant x \leqslant 0.4$). J. Alloy. Compd. **644**, 249 (2015)
7. Tazebay, A.S., Yi, S.I., Lee, J.K., Kim, H., Bahk, J.H., Kim, S.L., Park, S.D., Lee, H.S., Shakouri, A., Yu, C.: Thermal transport driven by extraneous nanoparticles and phase segregation in nanostructured Mg_2(Si, Sn) and estimation of optimum thermoelectric performance. ACS Appl. Mater. Interfaces **8**, 7003 (2016)
8. Liu, W., Tan, X.J., Yin, K., Liu, H.J., Tang, X.F., Shi, J., Zhang, Q.J., Uher, C.: Convergence of conduction bands as a means of enhancing thermoelectric performance of n-type $Mg_2Si_{1-x}Sn_x$ solid solutions. Phys. Rev. Lett. **108**, 166601 (2012)
9. Kim, G., Lee, H., Kim, J., Roh, J.W., Lyo, I., Kim, B.W., Lee, K.H., Lee, W.: Enhanced fracture toughness of Al and Bi co-doped Mg_2Si by metal nanoparticle decoration. Ceram. Int. **43**, 12979 (2017)
10. Kim, G., Lee, H., Rim, H.J., Kim, J., Kim, K., Roh, J.W., Choi, S.M., Kim, B.W., Lee, K.H., Lee, W.: Dependence of mechanical and thermoelectric properties of Mg_2Si-Sn nanocomposites on interface density. J. Alloy. Compd. **769**, 53 (2018)
11. Kim, G., Kim, S.W., Rim, H.J., Lee, H., Kim, J., Roh, J.W., Kim, B.W., Lee, K.H., Lee, W.: Improved trade-off between thermoelectric performance and mechanical reliability of Mg_2Si by hybridization of few-layered reduced graphene oxides. Scr. Mater. **162**, 402 (2019)
12. Kim, G., Rim, H.J., Lee, H., Kim, J., Roh, J.W., Lee, K.H., Lee, W.: Mg_2Si-based thermoelectric compounds with enhanced fracture toughness by introduction of dual nanoinclusions. J. Alloy. Compd. **801**, 234 (2019)
13. Kim, G., Lee, H., Kim, J., Roh, J.W., Lyo, I., Kim, B.W., Lee, K.H., Lee, W.: Up-scaled solid state reaction for synthesis of doped Mg_2Si. Scr. Mater. **128**, 53 (2017)
14. Kruzic, J.J., Ritchie, R.O.: Determining the toughness of ceramics from Vickers indentations using the crack-opening displacements: an experimental study. J. Am. Ceram. Soc. **86**, 1433 (2003)
15. Suh, D., Lee, S., Mun, H., Park, S.H., Lee, K.H., Kim, S.W., Choi, J.Y., Baik, S.: Enhanced thermoelectric performance of $Bi_{0.5}Sb_{1.5}Te_3$-expanded graphene composites by simultaneous modulation of electronic and thermal carrier transport. Nano Energy **13**, 67 (2015)
16. Nunna, R., Qiu, P., Yin, M., Chen, H., Hanus, R., Song, Q., Zhang, T., Chou, M.Y., Agne, M.T., He, J., Snyder, G.J., Shi, X., Chen, L.: Ultrahigh thermoelectric performance in Cu_2 Se-based hybrid materials with highly dispersed molecular CNTs. Energy Environ. Sci. **10**, 1928 (2017)
17. Zhang, Q., Zhou, Z., Dylla, M., Agne, M.T., Pei, Y., Wang, L., Tang, Y., Liao, J., Li, J., Bai, S., Jiang, W., Chen, L., Snyder, G.J.: Realizing high-performance thermoelectric power generation through grain boundary engineering of skutterudite-based nanocomposites. Nano Energy **41**, 501 (2017)
18. Zong, P., Hanus, R., Dylla, M., Tang, Y., Liao, J., Zhang, Q., Snyder, G.J., Chen, L.: Skutterudite with graphene-modified grain-boundary complexion enhances zT enabling high-efficiency thermoelectric device. Energy Environ. Sci. **10**, 183 (2017)
19. Walker, L.S., Marotto, V.R., Rafiee, M.A., Koratkar, N., Corral, E.L.: Toughening in graphene ceramic composites. ACS Nano **5**, 3182 (2012)
20. Satyala, N., Vashaee, D.: Detrimental influence of nanostructuring on the thermoelectric properties of magnesium silicide. J. Appl. Phys. **112**, 093716 (2012)
21. Satyala, N., Vashaee, D.: The effect of crystallite size on thermoelectric properties of bulk nanostructured magnesium silicide (Mg_2Si) compounds. Appl. Phys. Lett. **100**, 073107 (2012)
22. Zhao, L.D., Lo, S.H., He, J.Q., Li, H., Biswas, K., Androulakis, J., Wu, C.I., Hogan, T.P., Chung, D.Y., Dravid, V.P., Kanatzidis, M.G.: High performance thermoelectrics from earth-abundant materials: enhanced figure of merit in PbS by second phase nanostructures. J. Am. Chem. Soc. **133**, 20476 (2011)